

# Photogalvanic effects due to quantum interference in optical transitions demonstrated by terahertz radiation absorption in Si-MOSFETs

P. O. Ibrich,<sup>1</sup> S. A. Tarasenko,<sup>2</sup> C. Reitmaier,<sup>1</sup> J. Karch,<sup>1</sup> D. P. Lohmann,<sup>1</sup> Z. D. Kvon,<sup>3</sup> and S. D. Ganichev<sup>1</sup>

<sup>1</sup> Terahertz Center, University of Regensburg, 93040 Regensburg, Germany,

<sup>2</sup> A. F. Ioffe Physico-Technical Institute, Russian Academy of Sciences, 194021 St. Petersburg, Russia and

<sup>3</sup> Institute of Semiconductor Physics, Russian Academy of Sciences, 630090 Novosibirsk, Russia

(Dated: February 20, 2024)

We report on the observation of the circular (helicity-dependent) and linear photogalvanic effects in Si-MOSFETs with inversion channels. The developed microscopic theory demonstrates that the circular photogalvanic effect in Si structures is of pure orbital nature originating from the quantum interference of different pathways contributing to the light absorption.

PACS numbers:

The photogalvanic effects have been proved to be an efficient tool to study nonequilibrium processes in semiconductor structures yielding information on their symmetry, details of the band spin splitting, momentum, energy and spin relaxation times etc. (see e.g. [1, 2, 3, 4]). Microscopically, they are caused by the asymmetry of photoexcitation or relaxation processes and, thus, can be observed in a media of sufficiently low spatial symmetries only. The photogalvanic effects have recently been observed in a large class of low-dimensional structures for interband [5, 6, 7, 8] and intraband optical transitions [4, 9, 10].

Here we report on the observation of the circular (CPGE) and linear (LPGE) photogalvanic effect caused by absorption of THz radiation in Si-MOSFETs. The fact of the existence of the helicity-sensitive circular photogalvanic current, which reverses its direction upon switching the sign of circular polarization, in Si-based structures is of particular interest. So far, the CPGE has only been detected in materials with strong spin-orbit coupling and described by microscopic mechanisms based on spin-related processes [3, 4]. However, such mechanisms of the CPGE get ineffective in Si because of the vanishingly small constant of spin-orbit coupling and, therefore, can not account for the observed circular photocurrents. Thus, a new access in explaining the CPGE is required involving mechanisms of pure orbital (spin-unrelated) origin. Here, we show that the CPGE in our structures is due to quantum interference of different pathways contributing to light absorption [1] (see also [12, 13]). In contrast to the well known photocurrents caused by all-optical quantum interference of one- and two-photon absorption processes in a two-color light [14, 15, 16, 17], here the elementary one-photon absorption processes give rise to an electric current. Besides the CPGE, we also investigate the LPGE, which has so far been detected in Si-MOSFETs for direct intersubband transitions only [18]. Our results show that the free-carrier absorption also leads to the LPGE.

We study n-type MOSFETs prepared on monocrystalline Si surfaces. The surfaces of our samples are tilted by the an-

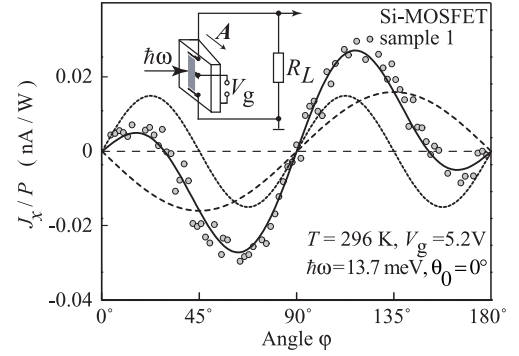


FIG. 1: Normalized photocurrent  $J_x/P$  measured in sample 1 as a function of the angle  $\phi$ . Full line is a fit to Eqs. (1). Dashed and dotted lines show the CPGE and LPGE contributions, respectively. The inset sketches the experimental set-up.

gle  $\theta = 9:7$  (sample 1) or  $\theta = 10:7$  (sample 2) from the (001) plane around  $x \parallel [110]$ . Two transistors oriented along and normal to the inclination direction  $A \parallel y$  with semitransparent Ti gates of 10 nm thickness are prepared on each substrate. Application of the gate voltage  $V_g = 1$  to 10 V enables us to change the carrier density  $N_s$  and the energy spacing  $\epsilon_{21}$  between the size-quantized subbands  $e1$  and  $e2$  in the range of  $N_s = 1.5$  to  $15 \cdot 10^{11} \text{ cm}^{-2}$  and  $\epsilon_{21} = 2$  to 20 meV, respectively. The peak electron mobility in the channel is about  $10^3$  and  $2 \cdot 10^4 \text{ cm}^2/\text{Vs}$  at  $T = 296$  and 4.2 K.

For optical excitation we applied THz radiation of a pulsed optically pumped  $\text{NH}_3$  laser [4]. The laser generates radiation pulses with a power  $P \approx 5 \text{ kW}$  and wavelengths  $\lambda = 76, 90.5$ , and  $148 \text{ nm}$  corresponding to the photon energies  $\hbar\omega = 16.3, 13.7$  and  $8.4 \text{ meV}$ , respectively. Quartz  $\theta = 4$  and  $\theta = 2$  plates were used to modify the laser light polarization. Rotating the  $\theta = 4$  plate by the angle  $\phi'$  between the plate optical axis and the incoming laser polarization we varied the radiation helicity as  $P_{\text{circ}} = \sin 2\phi'$ . By means of the  $\theta = 2$  plates we obtain the linearly polarized light with all possible angles between the electric field of radiation and the  $x$  axis. The photocurrents are measured between source and drain via

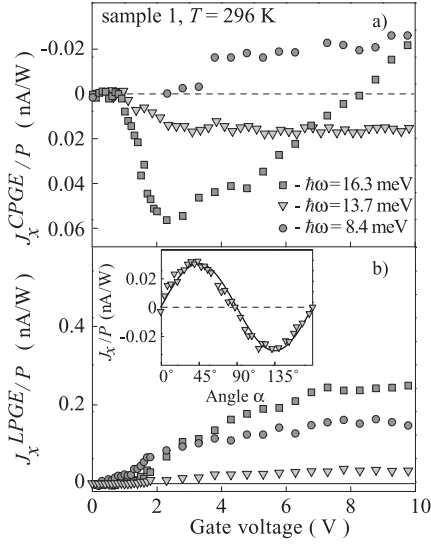


FIG. 2: Normalized photogalvanic currents as a function of the gate voltage. a) CPGE, b) LPGE. The inset shows the LPGE current as a function of the azimuth angle.

the voltage drop across a 50  $\Omega$  load resistor.

Irradiating MOSFET structures by polarized light at normal incidence, as sketched in the inset to Fig. 1, we observed a photocurrent signal with the temporal structure reproducing the laser pulse of about 100 ns duration. The signal is detected only for the gate voltages in the range of  $V_g = 1$  to 10 V. First we discuss data obtained at room temperature. Applying radiation to the transistors aligned perpendicular to  $A$  (see the inset in Fig. 1) and varying the radiation helicity, we observe that the induced photocurrent reverses its direction upon switching the radiation helicity from left- to right-handed circular polarization. In contrast, the photocurrent measured in transistors aligned along  $A$  is observed to be the same for both left- and right-handed circularly polarized light. The fact that the CPGE in miscut structures at normal incidence is observed only for the direction normal to  $A$  is in accordance with the phenomenological theory of the photogalvanic effects structures of the  $C_s$  point-group symmetry relevant to our miscut samples [9]. Our work is mostly devoted to the CPGE, therefore we focus below on this type of transistors only. Figure 1 shows the dependence of the photocurrent on the angle  $\theta'$  for radiation with  $\hbar\omega = 13.7$  meV measured for sample 1. The data can be well fitted by the equation [8, 4]

$$J(\theta') = J_C \sin 2\theta' + (J_L/2) \sin 4\theta' : \quad (1)$$

Here, the first and the second terms describe the CPGE and LPGE contribution to the photocurrent. Figure 1 shows substantial contribution of the CPGE to the total current. This feature persists for all gate voltages and all photon energies used in our experiments.

Figure 2a shows the dependences of the CPGE contributions  $J_C$  to the total photocurrent measured as a

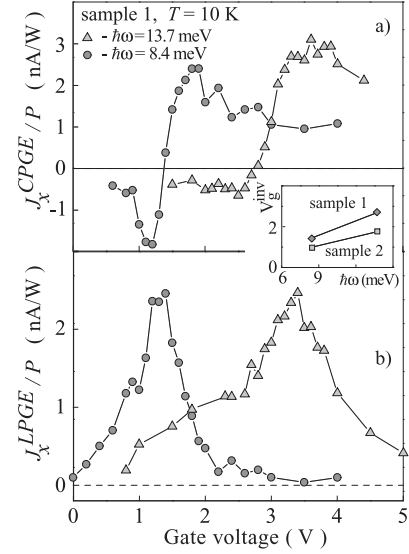


FIG. 3: Normalized circular photogalvanic current (a) and linear photogalvanic current (b) as a function of the gate voltage. The inset shows the spectral dependence of the gate voltage corresponding to the sign inversion of the CPGE.

function of the gate voltage  $V_g$ . The CPGE contribution is obtained by taking the difference between photoresponses to the right- and left-handed radiation yielding the CPGE current  $J_C = [J(\theta' = 45^\circ) - J(\theta' = 135^\circ)]/2$ .

To investigate the LPGE contribution in more detail, we excited our samples with linearly polarized radiation which excludes the CPGE. The photocurrent can be well fitted by the phenomenological equation [4]

$$J(\theta) = J_L \sin 2\theta ; \quad (2)$$

with the same parameter  $J_L$  as used in Eq. (1). The dependence of the LPGE contribution on the gate voltage is shown in Figure 2b where  $J_L = [J(\theta = 45^\circ) - J(\theta = 135^\circ)]/2$  is plotted for several radiation photon energies.

As follows from Fig. 2b, the LPGE current has the same sign for all radiation photon energies used and its magnitude increases with the gate voltage. Such a dependence can be attributed to the increase of the electron density in the inversion channel and, therefore, the Drude absorption enhancement. The CPGE behaviour, in contrast, is more complicated (see Fig. 2a). We observe that the direction of the CPGE current is opposite for  $\hbar\omega = 8.4$  meV and 13.7 meV. Moreover, for  $\hbar\omega = 16.3$  meV the signal changes its sign with the bias voltage increase. We note that we can not attribute this gate voltage to any characteristic energy in the band structure.

At low temperatures the behaviour of the photocurrent upon variation of the radiation polarization remains the same. All data can be well fitted by Eqs. (1) and (2) with comparable magnitudes of  $J_C$  and  $J_L$  proving the presence of both, CPGE and LPGE. The gate voltage behaviour, however, changes drastically as demon-

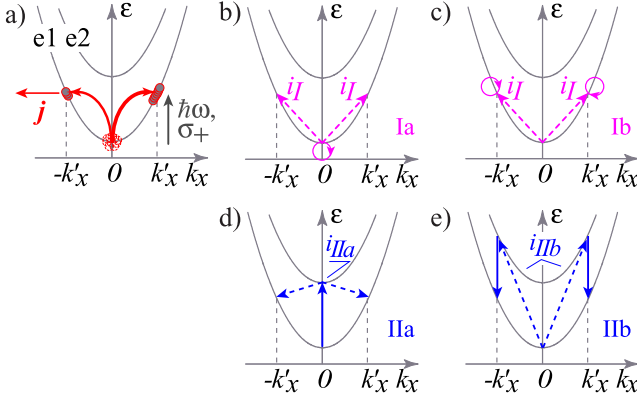


FIG. 4: Microscopic model of the CPGE. a) Indirect optical transitions due to absorption of circularly polarized light are shown by bend arrows of various thickness indicating the difference in transition rates for the absorption of circularly polarized radiation caused by the quantum interference of various pathways. Circles sketch the resulting imbalance of the carrier distribution yielding an electric current  $j$ . b) { e) Various pathways via intermediate states in the e1 and e2 subbands. Here, solid arrows indicate electron-photon interaction and the dashed arrows describe scattering events.

strated in Fig.3a for sample 1. The LPGE current, instead of smooth dependence observed at room temperature, shows a resonant response (see Fig.3b). The peak position depends on the photon energy and corresponds to the  $\hbar\omega = \epsilon_{21}$  subband separation. The resonance is obtained by tuning the band separation to the photon energy varying the gate voltage. Increasing of the photon energy should shift the intersubband resonance to the large gate voltages [19]. The position of the inter-subband resonance has been additionally proved by the photoconductive measurements in biased transistors. Note, that the difference in the resonance position for

fixed photon energy observed in sample 1 and 2 is attributed to the difference in the declination angle. In the CPGE we observe again the change of the current direction but, now, at all frequencies used. In contrast to the room temperature data, the gate voltage inversion at low temperatures takes place at the resonance  $\hbar\omega = \epsilon_{21}$ . In fact, the CPGE photocurrent changes its sign upon the gate voltage variation and vanishes at the gate voltage values at which the LPGE achieves its maximum (see Fig.3). The inset of Fig.3 shows the gate voltages of the CPGE inversion as a function of the photon energy.

The observation of the CPGE apart the inter-subband resonance demonstrates that the free carrier absorption of circularly polarized light gives rise to the helicity dependent current. Below we consider theoretically this process and show that the CPGE is caused by the interference of different pathways contributing to the radiation absorption. Figure 4a sketches the indirect optical transitions within the ground subband e1. Due to the energy and momentum conservation, the transitions

shown by bend arrows can only occur if the electron-photon interaction is accompanied by simultaneous electron scattering by phonons or static defects. Such optical transitions involving both the electron-photon interaction and electron scattering are treated as second-order virtual processes via intermediate states. Figure 4b { d shows possible absorption pathways with the intermediate states in the e1 and e2 subbands.

The dominant contribution to the D rude absorption involves intermediate states within the e1 subband. Such transitions (path I) are shown in Figs. 4b,d for the process where the electron-photon interaction is followed by electron scattering (Fig.4b) and the inverted sequence process (Fig.4d). The matrix element of the intra-subband optical transitions with intermediate states in the e1 subband on the vicinal silicon surface has the form [13, 19]

$$M_{k^0k}^{(1)} = \frac{eA}{c!} \frac{(\kappa_x^0 - k_x) e_x}{m_{xx}} + \frac{(\kappa_y^0 - k_y) e_y}{m_{yy}} V_{11}; \quad (3)$$

where  $e$  is the electron charge,  $A$  is the amplitude of the electromagnetic wave,  $\omega$  is the radiation frequency,  $m_{xx} = m_{\parallel}$  and  $m_{yy} = (m_{\parallel} \cos^2 \theta + m_{\perp} \sin^2 \theta)$  are the effective electron masses in the channel plane being different from each other due to the deviation of the channel plane from (001) by the angle  $\theta$ ,  $m_{\parallel}$  and  $m_{\perp}$  are the longitudinal and transverse effective masses in the valley in bulk Si,  $e = (e_x, e_y)$  is the unit vector of the light polarization and  $V_{11}$  is the matrix element of electron scattering within the subband e1. While the matrix element (3) is odd in the wave vector, the absorption probability given by the squared matrix element is even in  $(k^0 - k)$ . Thus, this type of processes alone does not introduce an asymmetry in the carrier distribution in  $k$ -space and, consequently, does not yield an electric current.

Pathways II via states in the e2 subband are sketched in Figs.4d,e. They involve virtual intersubband optical transitions which in miscut structures are allowed by selection rules even at normal incidence of radiation [12, 18, 19]. The matrix element of path II indirect optical transitions has the form

$$M_{k^0k}^{(2)} = 2i \frac{eA m_{zz}}{c \hbar m_{yz}} \frac{\hbar \omega \epsilon_{21} z_{21}}{(\hbar \omega)^2 - \epsilon_{21}^2} e_y V_{12}; \quad (4)$$

where  $1/m_{zz} = \cos^2 \theta / m_{\parallel} + \sin^2 \theta / m_{\perp}$ ,  $1/m_{yz} = (1/m_{\parallel} - 1/m_{\perp}) \cos \theta \sin \theta$  is the off-diagonal component of the reciprocal effective mass tensor,  $\epsilon_{21}$  is the energy separation between the subbands,  $z_{21}$  is the coordinate matrix element and  $V_{12}$  is the matrix element of intersubband scattering. Equation (4) shows that this type of indirect transitions is independent of  $k$  and, consequently, also does not lead to an electric current.

The photocurrent emerges due to the quantum interference of all virtual transitions considered above. Indeed, the total probability for the real optical transition

$k \neq k^0$  is given by the squared modulus of the sum of matrix elements describing individual pathways

$$|M_{k^0k}^{(1)}|^2 + |M_{k^0k}^{(2)}|^2 + 2\text{Re}(M_{k^0k}^{(1)}M_{k^0k}^{(2)}) : \quad (5)$$

Beside the probabilities of individual processes given by the first and the second term in the right-hand side of this equation, it contains the interference term. By using Eqs. (3) and (4) we derive for the latter term

$$\text{Re}(M_{k^0k}^{(1)}M_{k^0k}^{(2)}) / (k_x^0 - k_x) i(e_x e_y - e_x e_y) F(h!) : \quad (6)$$

This term is linear in the wave vector and, therefore, it results in different rates for the transitions to the positive and negative  $k_x^0$ . This, in turn, leads to an imbalance in the carrier distribution between  $k_x^0$  and  $-k_x^0$ , i.e., to an electric current  $j_k$ . Such a difference in the real optical transition rates caused by constructive or destructive interference of various pathways is illustrated in Fig. 4a. Moreover, the sign of the interference term is determined by the radiation helicity because  $i(e_x e_y - e_x e_y) = \hat{e}_z P_{\text{circ}}$ , where  $\hat{e}$  is a unit vector pointing along the light propagation direction [3, 4]. Therefore, the imbalance of the carrier distribution in  $k$ -space and, consequently, the photocurrent reverse upon switching the light helicity.

Equation (6) also explains the observed at low temperature inversion of the circular photocurrent direction when the energy separation between the subbands varies from  $\hbar\omega_{21} < h\omega$  to  $\hbar\omega_{21} > h\omega$ . Indeed, the interference term is proportional to the function  $F(h\omega) / 1 + [(h\omega)^2 - \hbar\omega_{21}^2]$ , which stems from the matrix element describing virtual transitions via the  $e2$  subband [see Eq. (4)]. In the vicinity of the intersubband absorption peak, the photocurrent increases drastically and undergoes spectral inversion. In real structures the dependence smooths because of the broadening, but the inversion remains. At room temperature, when the excited subbands  $e2$ ,  $e3$  etc., are also occupied in the equilibrium and considerably broaden, the inversion of the photocurrent does not couple to  $\hbar\omega_{21}$  anymore, as observed in experiment.

Assuming the electron scattering by short-range static defects, we write for the photocurrent [11, 13]

$$j = e \frac{8}{h} \sum_{k,k^0} X [v_p(k^0) v(k) - v_p(k) v(k^0)] [f(k) - f(k^0)] + 2\text{Re}(M_{k^0k}^{(1)}M_{k^0k}^{(2)}) (k^0 - k - \hbar\omega); \quad (7)$$

where  $v_p(k)$  is the momentum relaxation time,  $v_x(k) = \hbar k_x / m_{xx}$  and  $v_y(k) = \hbar k_y / m_{yy}$  are the velocity components,  $\epsilon_k$  is the electron kinetic energy measured from the subband bottom,  $f(k)$  is the function of equilibrium carrier distribution in the subband  $e1$ , and factor 8 in Eq. (7) accounts for the spin and valley degeneracy. Finally, we derive for the circular photocurrent density in Si MOSFET structures with a small declination angle

$$j_k = e \frac{m_k}{m_{yz}} \frac{\hbar V_{11} V_{12} i}{\hbar V_{11}^2 i} \frac{\epsilon_{21}^2 \epsilon_{21}^2}{\epsilon_{21}^2} \frac{\epsilon_x}{(h\omega)^2} \hat{e}_z I P_{\text{circ}}; \quad (8)$$

where  $\epsilon_x$  is the channel absorbance for the radiation polarized along the  $x$  axis,  $I$  is the radiation intensity, and the angle brackets stand for averaging over the spacial distribution of scatterers. Equation (8) describes the CPGE caused by the free carrier absorption at  $h\omega < \hbar\omega_{21}$  when the kinetic energy of photoexcited carriers is smaller than the intersubband spacing. For electrons with  $\epsilon_k > \hbar\omega_{21}$  the momentum relaxation time gets shorter because of the additional relaxation channel caused by the intersubband scattering. Consequently, the magnitude of the current is smaller for  $h\omega > \hbar\omega_{21}$  (low  $V_g$ ) than that at  $h\omega < \hbar\omega_{21}$  (large  $V_g$ ). This can be responsible for the observed asymmetry in the gate voltage dependence of the photocurrent in the intersubband resonant vicinity, see Fig. 3a. At  $h\omega \approx \hbar\omega_{21}$ , possible contributions to the CPGE due to the intersubband optical transitions as well as the scattering-induced broadening of the absorption peak should also be taken into account [12].

The magnitude of the CPGE current detected in sample 1 for  $h\omega = 8.4 \text{ meV}$  and  $V_g = 3 \text{ V}$  is  $J_x = P = 1 \text{ nA/W}$ , yielding the current density  $j_k = I = 0.1 \text{ nA/cm}^2$ . The same order of magnitude is obtained from Eq. (8) for the structure with the vicinal angle  $\theta = 9.7^\circ$ , the carrier density  $N_s = 5 \cdot 10^{11} \text{ cm}^{-2}$  ( $V_g = 3 \text{ V}$ ), the channel width  $a = 80 \text{ \AA}$  and the structure asymmetry degree  $\theta = 10^{-2}$ .

To summarize, we demonstrate in experiments on Si-based structures that the photon helicity-dependent photocurrents can be generated in low-dimensional semiconductor even with vanishingly small spin-orbit interaction. The mechanism of the photocurrent formation is based on the quantum interference of different pathways contributing to the radiation absorption.

We thank E. L. Ivchenko, V. V. Bel'kov, L. E. Golub and S. N. Danilov. The financial support from the DFG and the RFBR is gratefully acknowledged.

- 
- [1] B. I. Sturman and V. M. Fridkin, *The Photovoltaic and Photorefractive Effects in Non-Centrosymmetric Materials* (Nauka, Moscow, 1992; Gordon and Breach, New York, 1992).
  - [2] P. Reimann, *Physics Reports* 361, 57 (2002).
  - [3] E. L. Ivchenko, *Optical spectroscopy of semiconductor nanostructures* (Alpha Science International, Harrow, UK, 2005).
  - [4] S. D. Ganichev and W. Prettl, *Intense Terahertz Excitation of Semiconductors* (Oxford University Press, 2006).
  - [5] V. V. Bel'kov et al, *Solid State Commun.* 128, 283 (2003).
  - [6] M. Biele et al, *Appl. Phys. Lett.* 86, 061102 (2005).
  - [7] C. L. Yang et al, *Phys. Rev. Lett.* 96, 186605 (2006).
  - [8] K. S. Cho et al, *Appl. Phys. Lett.* 90, 041909 (2007).
  - [9] S. D. Ganichev et al, *Phys. Rev. Lett.* 86, 4358 (2001).
  - [10] S. D. Ganichev et al, *Phys. Rev. B* 68, 081302 (2003).
  - [11] S. A. Tarasenko, *Pis'ma Zh. Eksp. Teor. Fiz.* 85, 216 (2007) [*JETP Lett.* 85, 182 (2007)].
  - [12] L. I. M. Agarril and M. V. Entin, *Fiz. Tverd. Tela* 31 (8), 37

- (1989) [Sov. Phys. Solid State 31, 1299 (1989)].
- [13] E.L.Ivchenko and G.E.Pikus, Superlattices and Other Heterostructures (Springer-Verlag, Berlin, 1997).
- [14] M.V.Entin, Fiz. Tekh. Poluprovodn. 23, 1066 (1989) [Sov. Phys. Semicond. 23, 664 (1989)].
- [15] A.Hache et al, Phys. Rev. Lett. 78, 306 (1997).
- [16] R.D.R.Bhat, and J.E.Sipe, Phys. Rev. Lett. 85, 5432 (2000).
- [17] M.J.Stevens et al, J. Appl. Phys. 91, 4382 (2002).
- [18] G.M.Gusev et al, Pisma Zh. Eksp. Teor. Fiz. 46, 28 (1987) [JETP Lett. 46, 33 (1987)].
- [19] T.Ando, A.B.Fowler, and F.Stem, Rev. Mod. Phys. 54, 437 (1982).